TASK QUARTERLY 5 No 1 (2001), 29–58

WIND- AND DENSITY-DRIVEN WATER CIRCULATION IN THE SOUTHERN BALTIC SEA: A NUMERICAL ANALYSIS

AGNIESZKA HERMAN[1] AND ANDRZEJ JANKOWSKI[2]

[1]*Department of Physical Oceanography,*
Faculty of Biology, Geography and Oceanography,
University of Gdansk,
Al. Piłsudskiego 46, 81-378 Gdynia, Poland
herman@ocean.univ.gda.pl

[2]*Institute of Oceanology,*
Polish Academy of Sciences,
Powstańców Warszawy 55, 81-712 Sopot, Poland
jankowsk@ocean.iopan.gda.pl

(Received 10 May 2000; revised manuscript received 28 June 2000)

Abstract: The study focuses on the hydrodynamic processes in the southern Baltic Sea, with special interest in the Stolpe Channel – the only deep water connection between Bornholm Basin to the west and Gdansk and Gotland Basins to the east. The Channel is an area of strong interactions of wind- and density-driven currents that may lead to a complex flow structure. A three-dimensional numerical model was applied to an analysis of processes mentioned above. Three model versions of different spatial resolution (5, 3 and 1Nm) were used to investigate an influence of this parameter on the model results. The simulations were performed for four main wind directions, for a variable in time wind speed. It was shown that water circulation in the southern Baltic is to a high degree dependent on local anemobaric conditions. The results confirm the hypothesis of Krauss and Brügge that the flow in the Channel is opposite to the wind direction. Numerical grid step can have a decisive influence on the modeled circulation patterns, especially when barotropic and baroclinic flow components counteract. In such situations – when the flow is bidirectional and mesoscale eddies are generated – high resolution of the model is particularly important.

Keywords: wind-driven circulation, density currents, hydrodynamic modeling, Stolpe Channel, southern Baltic, Princeton Ocean Model

Symbol conventions

A_1, A_2	empirical constants in the turbulence model
A_H	horizontal heat diffusivity
A_M	horizontal kinematic viscosity
B_1, B_2	empirical constants in the turbulence model
C_1	empirical constant in the turbulence model
C	the coefficient of the Smagorinsky diffusivity
C_z	bottom stress coefficient

c_n	wavespeed perpendicular to the model boundary
c_s	sound speed in water
D	total water depth ($D = H + \eta$)
E_1, E_2, E_3	empirical constants in the turbulence model
$F_{q^2}, F_{q^2\ell}$	horizontal diffusion in the turbulence model
F_S	horizontal diffusion of salt
F_T	horizontal diffusion of heat
F_x, F_y	components of horizontal diffusion along x and y axis, respectively
f	Coriolis parameter
G_H	Richardson number
G_M	nondimensional coefficient in the turbulence model
g	acceleration due to gravity
H	water depth
K_H	vertical diffusivity of heat and salt
K_M	vertical kinematic viscosity
K_q	vertical turbulent viscosity
k	von Kármán constant
kb	number of sigma-levels in the model
L_{FRS}	the width of the FRS zone
n	direction perpendicular to the model boundary
Pr	inverse Prandtl number
p	hydrostatic pressure
q^2	twice the turbulent kinetic energy
R	radiation
S	salinity
S_H, S_M, S_q	stability function in the turbulence model
T	temperature
t	time
U, V	components of velocity vector, along x and y axis, respectively
$U_{\tau,0}, V_{\tau,-1}$	surface and bottom (respectively) stress velocities
$\bar{U}, \bar{V}$	vertically averaged velocity vector components
$\tilde{W}$	wall proximity function
w	vertical component of velocity vector
x, y	horizontal coordinates
z	Cartesian vertical coordinate
z_0	roughness parameter
α	weight function in FRS boundary model
Δt_e	external mode time step
Δt_i	internal mode time step
$\Delta x, \Delta y$	grid spacing along x and y axis, respectively
$\Delta\sigma$	grid spacing along the vertical axis
η	free surface elevation
ρ	water density
ρ_0	average water density
ρ_a	air density
σ	scaled vertical coordinate
τ_x, τ_y	surface wind stress components
ω	velocity component perpendicular to σ-surfaces
ℓ	the turbulence length scale

1. Introduction

One of the first problems one has to deal with when applying a numerical model to an analysis of hydrodynamic processes in a real water basin is the choice of spatial and time resolution of the model. The choice is usually a compromise between available computer power and time and – on the other hand – precision, with which one wants to simulate processes taking place in nature. The minimal resolution required to obtain a given precision is usually very difficult – or even impossible – to define, because of a variety of processes shaping the circulation in a particular water body. These processes interact with each other in a very complicated way; small-scale processes (like meanders, eddies *etc.*) are under influence of global circulation structures, but (which is often ignored for practical reasons) they can also affect significantly the large-scale dynamics (for example the energy of mesoscale eddies is often big enough so that it contributes to the global circulation).

The area which was the subject of investigation in this work was the southern part of the Baltic Sea, with special interest in the Stolpe Channel – an oblong bottom structure, which is the only deep-water connection between the Bornholm Basin to the west and the Gdansk Basin and Gotland Basin to the east. A detailed description of hydrological conditions in this area and processes shaping the circulation can be found in the next section.

The purpose of this study was, firstly, to describe wind- and density-driven water transport in the bottom and surface layers in the region mentioned above, and secondly, to find an answer to the question how and to what degree spatial resolution of the model influences the results, provided the other parameters remain unchanged. All calculations were carried out by means of the Princeton Ocean Model, a description of which can be found in Section 3. In Sections 4 and 5 the diagnostic and prognostic calculations are described, together with an analysis of the results.

2. Hydrological conditions in the Baltic Sea

The Baltic Sea is a shallow (mean depth 52 m) inland sea, the main feature of which is a very complicated bottom topography (Figure 1) and a huge watershed, much bigger than the surface of the sea itself (1.7 mln km^2 and 400000 km^2, respectively). Intensive input of fresh water from the surrounding land leads to high discharges of natural and anthropogenic substances, as well as to decrease of water salinity in northern and eastern parts of the Sea. Together with sea water inflows through the Danish Straits this results in considerable horizontal salinity gradients and great diversity of biogeochemical conditions in each particular subbasin [1, 2]. Limited water exchange between the subbasins is caused by two most important factors, namely a specific bottom topography (deep basins separated by shoals and sills), which restrains horizontal circulation, and a very high vertical density gradient, which limits vertical water movements. The halocline is of permanent character and is not affected even in periods of strong autumn mixing. Vertical water exchange is additionally weakened by a seasonal thermocline, the maximum development of which takes place during the summer. The processes listed above lead to stagnation and oxygen depletion in bottom water masses. The only process allowing water exchange below the halocline are inflows of salty, highly oxygenated waters from the North Sea. Such inflows are of random, episodic character; their intensity and frequency depends on many different factors, connected with each other in a complicated way. Thus, in all Baltic Sea subbasins

alternately occurring periods of stagnation and water exchange can be observed. For example, after a three-week-long period of westerly winds in January 1993, over 300 km^3 of high salinity water were transported to the western parts of the Baltic [3]. The event interrupted 16-year period of stagnation, during which in the Gotland and Gdansk Deep the highest concentrations of hydrogen sulphide ever observed occurred [1, 2, 4].

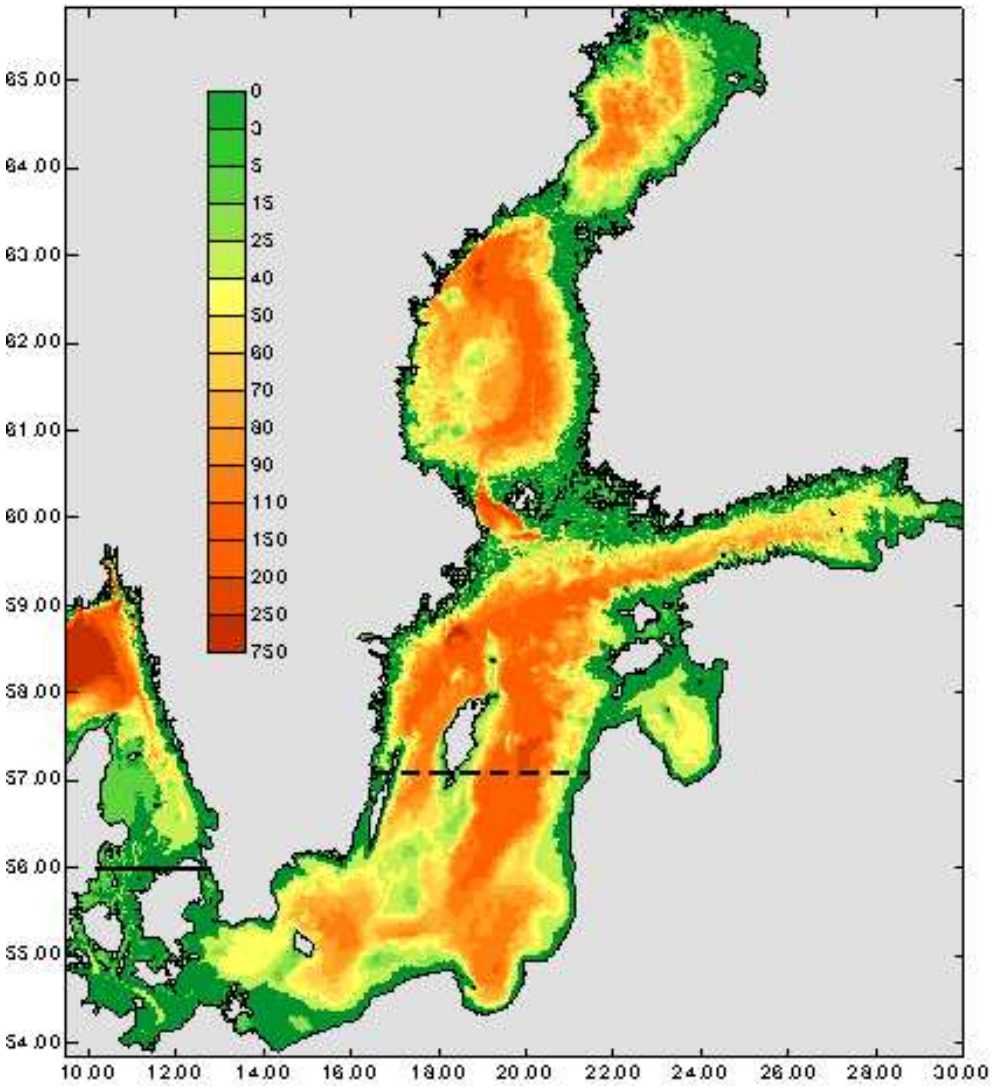

Figure 1. Bottom topography of the Baltic Sea (on the basis of data from the Institut für Ostseeforschung, Warnemünde [19]). Solid line – the boundary of the model in the Danish Straits; dashed line – the boundary of Model **MA** (see Section 3.3)

inflow resulted in deep water exchange in all basins of the Sea. In the Arkona Basin the 16 PSU isohaline was shifted from the depth of 90 meters to 70 meters; salinity in the Bornholm Basin, in its deepest part, increased from 15 to 20 PSU, and the oxygen concentration from

1 to 7.5 cm^3/dm^3; salinity in the Stolpe Channel increased from 10 to about 15 PSU. In the summer of 1993 the salty waters reached northern parts of the Gotland Deep.

Because of the important consequences of salt water inflows for the environment of the Baltic Sea, many efforts are taken to understand the processes that influence spreading of inflow waters – the research is run experimentally by measurements of currents and physico-chemical properties of the water, as well as by means of hydrodynamic and ecological models. The investigations concentrate on two main groups of problems. The first one is an analysis of conditions which must be fulfilled so that salty waters from the Kattegat can penetrate through the Danish Straits to the Baltic (*e.g.* [3–6]); the second group of problems – which is also the main purpose of this study – relates to the mechanisms of the transport of water to the successive subbasins of the Baltic Proper (*e.g.* [7–10]). In both cases an episodic character of the phenomena analyzed is a serious difficulty. The measurements are often not representative for longer periods of time or bigger regions. On the other hand, necessity of taking into account processes of big extent of spatial and time scales is also a challenge for modern numerical models [5]. The processes which take part in shaping water circulation are of different importance in different seasons and regions, and are connected with each other in a complicated way. Thus, small approximations may lead to significant changes in modeled results. A good example is the Danish Straits region, where flow is mainly generated by sea level difference between the Kattegat and south-east Baltic. This is the reason why barotropic models of flow through the Straits are very often used – such models allow to estimate in a simple way water transport close to its real values and simulate the most characteristic features of the flow [11], but they contain too little information to reproduce detailed three-dimensional structure of water masses and of the flow itself. It has been proved that unidirectional flow through the Danish Straits, which is an effect of barotropic models, occurs relatively rarely, only when the sea level differences are very big. The real circulation is a complicated superposition of barotropic and baroclinic processes, particularly in situations when they act in opposite directions. These conclusions are of universal character and can be applied to other parts of the Baltic Sea as well, *e.g.* to the Bornholm Channel or the Stolpe Channel. In the Bornholm Channel a very interesting phenomenon of wind current counteracting density current has been observed during periods of strong westerly winds. Similar processes can also occur in the coastal zone, where they lead to weakening or intensification of coastal jets [12].

An important parameter, which decides on the character of flow between subbasins of the Baltic, is a ratio of halocline depth to the depth of the sill separating the two given subbasins. This parameter influences not only the transport of deep, salty waters, but also intensity of turbulent mixing, mesoscale eddies generation, internal waves and other processes connected with flow instability. In the case of the Stolpe Channel the halocline depth is approximately equal to the sill depth (60 m); this can be regarded as an explanation to the fact that the Stolpe Channel is one of the three main regions of mixing in the Baltic (together with the Belt Sea and Arkona Basin). An entrainment rate for this area (defined as an uptake of low density water in the deep gravity transport) has been estimated to about 28% [13]. For comparison, in the Bornholm Channel it is almost equal zero.

A more detailed description of hydrodynamic processes in the Southern Baltic can be found in Sections 4 and 5, together with an analysis of the model results.

3. Model description

All numerical experiments described in the following sections have been carried out with the Princeton Ocean Model (POM) – a three-dimensional, baroclinic hydrodynamic model, which is (in many different versions) widely used all over the world to investigate various dynamic processes taking place in coastal areas, as well as in the open ocean.

The model is based on vertically scaled coordinates, so-called σ-coordinates (Figure 2). This implies that the number of layers is the same all over the model domain, independently of water depth. All model equations have been transformed from the "traditional" z-coordinates to the new coordinate system according to the formula:

$$\sigma = \frac{z-\eta}{H+\eta} = \frac{z-\eta}{D},$$

where η denotes the free surface elevation, H – water depth and $D = H+\eta$. Thus, σ ranges from 0 on the free surface to -1 at the bottom.

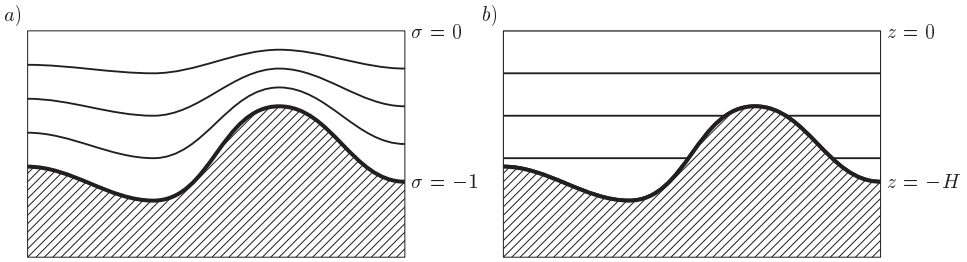

Figure 2. Two kinds of vertical coordinates used in ocean models: σ-coordinates (a) and cartesian coordinates (b)

3.1. Basic equations

Basic equations of the Princeton Ocean Model are equations of motion [14]:

$$\frac{\partial UD}{\partial t} + \frac{\partial U^2 D}{\partial x} + \frac{\partial UVD}{\partial y} + \frac{\partial U\omega}{\partial \sigma} - fVD + \\ + gD\frac{\partial \eta}{\partial x} + \frac{gD^2}{\rho_0}\int_\sigma^0 \left(\frac{\partial \rho'}{\partial x} - \frac{\sigma'}{D}\frac{\partial D}{\partial x}\frac{\partial \rho'}{\partial \sigma'}\right) d\sigma' = \frac{\partial}{\partial \sigma}\left(\frac{K_M}{D}\frac{\partial U}{\partial \sigma}\right) + F_x, \tag{1.1}$$

$$\frac{\partial VD}{\partial t} + \frac{\partial UVD}{\partial x} + \frac{\partial V^2 D}{\partial y} + \frac{\partial V\omega}{\partial \sigma} + fUD + \\ + gD\frac{\partial \eta}{\partial y} + \frac{gD^2}{\rho_0}\int_\sigma^0 \left(\frac{\partial \rho'}{\partial y} - \frac{\sigma'}{D}\frac{\partial D}{\partial y}\frac{\partial \rho'}{\partial \sigma'}\right) d\sigma' = \frac{\partial}{\partial \sigma}\left(\frac{K_M}{D}\frac{\partial V}{\partial \sigma}\right) + F_y, \tag{1.2}$$

continuity equation:

$$\frac{\partial DU}{\partial x} + \frac{\partial DV}{\partial y} + \frac{\partial \omega}{\partial \sigma} + \frac{\partial \eta}{\partial t} = 0, \tag{2}$$

and transport equations for heat and salt:

$$\frac{\partial TD}{\partial t} + \frac{\partial TUD}{\partial x} + \frac{\partial TVD}{\partial y} + \frac{\partial T\omega}{\partial \sigma} = \frac{\partial}{\partial \sigma}\left(\frac{K_H}{D}\frac{\partial T}{\partial \sigma}\right) + F_T - \frac{\partial R}{\partial z}, \tag{3.1}$$

$$\frac{\partial SD}{\partial t} + \frac{\partial SUD}{\partial x} + \frac{\partial SVD}{\partial y} + \frac{\partial S\omega}{\partial \sigma} = \frac{\partial}{\partial \sigma}\left(\frac{K_H}{D}\frac{\partial S}{\partial \sigma}\right) + F_S. \tag{3.2}$$

POM includes also a sub-model which describes turbulent processes. It is based on the following set of equations [15]:

$$\frac{\partial q^2 D}{\partial t}+\frac{\partial U q^2 D}{\partial x}+\frac{\partial V q^2 D}{\partial y}+\frac{\partial \omega q^2}{\partial \sigma}=\frac{\partial}{\partial \sigma}\left(\frac{K_q}{D}\frac{\partial q^2}{\partial \sigma}\right)+$$
$$+\frac{2K_M}{D}\left[\left(\frac{\partial U}{\partial \sigma}\right)^2+\left(\frac{\partial V}{\partial \sigma}\right)^2\right]+\frac{2g}{\rho_0}K_H\frac{\partial \tilde{\rho}}{\partial \sigma}-\frac{2Dq^3}{B_1\ell}+F_{q^2}, \tag{4.1}$$

$$\frac{\partial q^2 \ell D}{\partial t}+\frac{\partial U q^2 \ell D}{\partial x}+\frac{\partial V q^2 \ell D}{\partial y}+\frac{\partial \omega q^2 \ell}{\partial \sigma}=\frac{\partial}{\partial \sigma}\left(\frac{K_q}{D}\frac{\partial q^2 \ell}{\partial \sigma}\right)+$$
$$+E_1\ell\left(\frac{K_M}{D}\left[\left(\frac{\partial U}{\partial \sigma}\right)^2+\left(\frac{\partial V}{\partial \sigma}\right)^2\right]+E_3\frac{g}{\rho_0}K_H\frac{\partial \tilde{\rho}}{\partial \sigma}\right)\tilde{W}+F_{q^2\ell}, \tag{4.2}$$

where:

$$\tilde{W}=1+E_2\left[\frac{\ell}{k}\left((\eta-z)^{-1}+(H-z)^{-1}\right)\right]^2$$

and

$$\frac{\partial \tilde{\rho}}{\partial \sigma}=\frac{\partial \rho}{\partial \sigma}-c_s^{-2}\frac{\partial p}{\partial \sigma}.$$

The coefficients K_q, K_H, K_M depend on the stability functions S_q, S_H, S_M. S_q is a constant equal 0.20; the values of S_H and S_M are determined from the set of equations:

$$A_2=S_M(6A_1A_2G_M)+S_H(1-2A_2B_2G_H-12A_1A_2G_H),$$
$$A_1(1-3C_1)=S_M\left(1+6A_1^2G_M+9A_1A_2G_H\right)-S_H\left(12A_1^2G_H+9A_1A_2G_H\right),$$
$$G_M=\frac{\ell^2}{q^2}\sqrt{\left(\frac{\partial u}{\partial z}\right)^2+\left(\frac{\partial v}{\partial z}\right)^2},$$
$$G_H=\frac{\ell^2}{q^2}\frac{g}{\rho_0}\frac{\partial p}{\partial z}.$$

The non-dimensional coefficients A_1, A_2, B_1, B_2, C_1, E_1, E_2 and E_3 have been determined in the laboratory experiments and their values are: $A_1=0.92$, $A_2=0.74$, $B_1=16.6$, $B_2=10.1$, $C_1=0.08$, $E_1=1.8$, $E_2=1.33$ and $E_3=1.0$.

Water density was calculated as a function of salinity and temperature on the basis of the UNESCO formula [16], modified to minimize computational memory needed.

The expressions F_x and F_y in Equations (1) describe horizontal diffusion and are calculated according to the formulas:

$$F_x=\frac{\partial}{\partial x}\left(2A_MH\frac{\partial U}{\partial x}\right)+\frac{\partial}{\partial y}\left(A_MH\left(\frac{\partial U}{\partial y}+\frac{\partial V}{\partial x}\right)\right),$$
$$F_y=\frac{\partial}{\partial x}\left(A_MH\left(\frac{\partial U}{\partial y}+\frac{\partial V}{\partial x}\right)\right)+\frac{\partial}{\partial y}\left(2A_MH\frac{\partial V}{\partial y}\right).$$

The form of these formulas enables a proper description of bottom boundary layer (it is important because of high values of horizontal diffusion in this layer). The expressions F_T, F_S, F_{q^2} and $F_{q^2\ell}$ in Equations (3) and (4) have an analogous form to the one written above:

$$F_\Psi=\frac{\partial}{\partial x}\left(A_HH\frac{\partial \Psi}{\partial x}\right)+\frac{\partial}{\partial y}\left(A_HH\frac{\partial \Psi}{\partial y}\right),$$

where Ψ denotes T, S, q^2 or $q^2\ell$. The coefficients A_H and A_M, according to Smagorinsky formula, are functions of spatial resolution of the model and horizontal velocity gradient:

$$A_M = C\Delta x\Delta y\left[\left(\frac{\partial u}{\partial x}\right)^2+\frac{1}{2}\left(\frac{\partial v}{\partial x}+\frac{\partial u}{\partial y}\right)^2+\left(\frac{\partial v}{\partial y}\right)^2\right]^{\frac{1}{2}},$$

$$A_H = Pr\cdot A_M.$$

It is clear that the value of A_M decreases with an increased resolution of the model and is very small when the velocity gradients are small. The non-dimensional coefficient C was set to 0.20.

3.2. Boundary conditions

Free surface boundary conditions for the model governing equations have been defined as follows:

$$\rho_0\frac{K_M}{D}\frac{\partial U}{\partial\sigma}=\tau_x,\qquad \rho_0\frac{K_M}{D}\frac{\partial V}{\partial\sigma}=\tau_y,\qquad \rho_0\frac{K_H}{D}\frac{\partial S}{\partial\sigma}=0,$$

$$q^2 = B_1^{2/3}U_{\tau,0}^2 \qquad \text{and} \qquad q^2\ell = 0.$$

The values of temperature in the surface layer were interpolated from the climatic data representative for a given season.

The bottom ($\sigma=-1$) boundary conditions are:

$$\omega = 0,$$

$$\frac{K_M}{D}\frac{\partial U}{\partial\sigma}=C_z U\sqrt{U^2+V^2},\qquad \frac{K_M}{D}\frac{\partial V}{\partial\sigma}=C_z V\sqrt{U^2+V^2},$$

$$\frac{K_H}{D}\frac{\partial T}{\partial\sigma}=0,\qquad \frac{K_H}{D}\frac{\partial S}{\partial\sigma}=0,$$

$$q^2 = B_1^{2/3}U_{\tau,-1}^2 \qquad \text{and} \qquad q^2\ell = 0.$$

The coefficient C_z depends on the thickness of the bottom layer of the model:

$$C_z = \max\left\{\frac{k^2}{\ln^2\left((1+\sigma_{kb-1})\,H/z_0\right)}, 0.0025\right\}.$$

The von Kármán constant equals 0.4 and $z_0 = 0.01$ m.

On closed (land) boundaries the velocity vector components perpendicular to the wall were set to zero.

In the model there were two kinds of open boundaries. In the Danish Straits, in all three versions of the model (see below), the component of velocity vector perpendicular to the boundary was calculated by means of the radiation condition [17]:

$$\frac{\partial U_n}{\partial t}+c_n\frac{\partial U_n}{\partial n}=0 \qquad \text{and} \qquad H\bar{U}_n+\sqrt{gH}\,\eta=0,$$

where n means the direction perpendicular to the boundary. An assumption was made that the velocity component tangent to the boundary vanishes. In the case of temperature and salinity the following conditions were fulfilled:

$$\frac{\partial T}{\partial t}+U_n\frac{\partial T}{\partial n}=0 \qquad \text{and} \qquad \frac{\partial S}{\partial t}+U_n\frac{\partial S}{\partial n}=0.$$

In the case of Model **MA** there was a necessity of defining boundary conditions for the northern boundary; they were calculated on the basis of the results of Model **MB** by

means of the FRS (Flow Relaxation Scheme) method. This technique is based on so-called FRS zones, within of which values of modeled parameter Φ are estimated as a weighted average of external solution Φ_e and internal solution Φ_i (Figure 3):

$$\Phi = \alpha \Phi_e + (1-\alpha)\,\Phi_i,$$

where $\alpha \equiv \alpha(x, y)$ varies from 0 on the internal boundary of the FRS zone ($\Phi = \Phi_i$), to 1 on the external boundary ($\Phi = \Phi_e$). There does not exist a method for finding an optimal shape for α function. In the described model a quite popular quadratic form was chosen [17]:

$$\alpha(x) = \left(1 - \frac{x}{L_{FRS}}\right)^2, \qquad 0 < x < L_{FRS}$$

(in the case of a western boundary). L_{FRS} denotes the width of the FRS zone, expressed as a multiple of numerical grid step: $L_{FRS} = N \cdot \Delta x$, where N was set to 9.

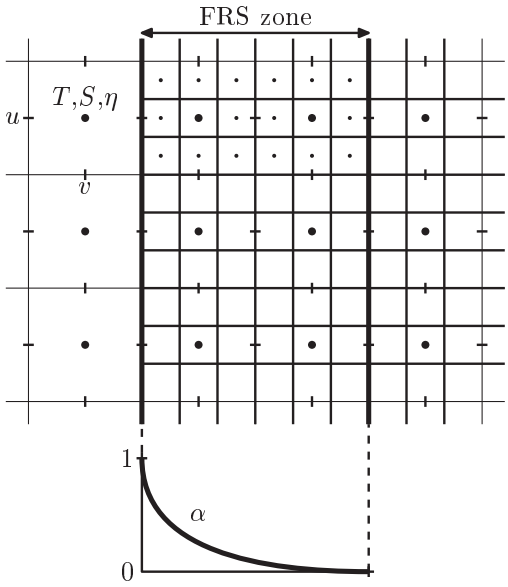

Figure 3. A scheme of an open boundary based on the FRS technique. In the FRS zone each variable is calculated as a weighted average (with weight function α) of internal solution (obtained from high resolution model) and external solution (obtained from a coarse resolution model). For greater clearness of the picture not all grid points are plotted ([30], modified)

An advantage of the FRS technique is that it allows a proper description of velocity field not only near outflow boundaries, but also near the boundaries where the flow is directed towards the interior of the modeled domain. FRS zones allow also to filter out noise from an external solution Φ_e. The smaller the difference between an external and internal solutions and the wider the FRS zone, the more reliable the results are [18].

3.3. Numerical scheme

POM is a free surface model, which implies that existence of high frequency gravity waves makes it necessary to use small time step, according to the CFL (*Courant–Friedrichs–*

Levy) condition:

$$\Delta t_e \leq \frac{1}{2\sqrt{gH}} \left(\frac{1}{(\Delta x)^2} + \frac{1}{(\Delta y)^2} \right)^{-1/2}.$$

Such temporal resolution requires very big computational costs. The solution to this problem is a so-called *mode splitting* – the equations are split into vertically integrated barotropic

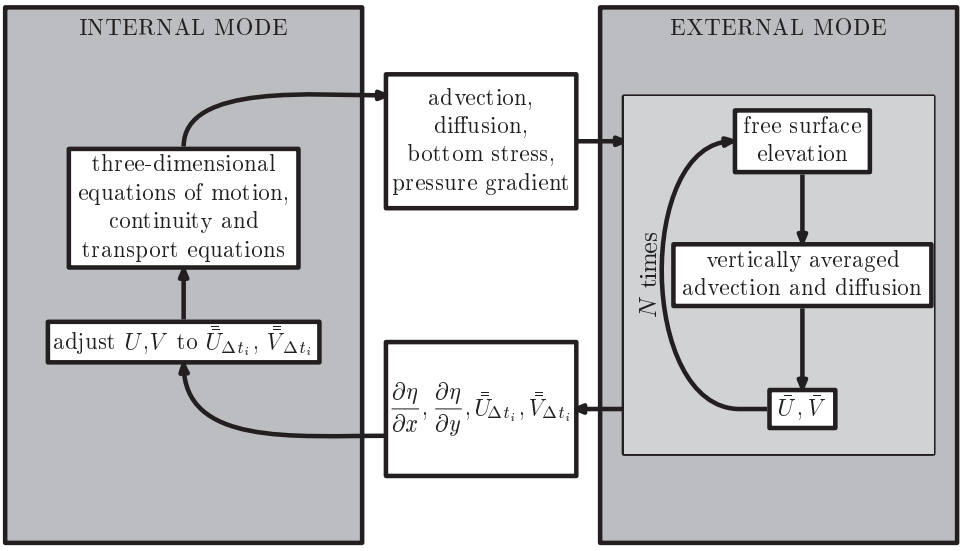

Figure 4. Mode splitting. Interactions between the baroclinic (internal mode) and barotropic (external mode) part of the model. N is an integer equal to $\Delta t_i / \Delta t_e$

equations and baroclinic equations (Figure 4). Barotropic equations, solved with a shorter time step Δt_e, are based on depth-averaged velocity components:

$$\bar{U} = \frac{1}{H+\eta} \int_{-1}^{0} U d\sigma \qquad \text{and} \qquad \bar{V} = \frac{1}{H+\eta} \int_{-1}^{0} V d\sigma.$$

Baroclinic equations, integrated with a much longer time step Δt_i, provide expressions required to solve the barotropic part of the model, namely: vertically integrated velocity gradient together with advection and diffusion terms. Free surface elevation gradient is passed on in the opposite direction.

The numerical grid used is Arakawa C grid (Figure 5).

The calculations were carried out for three different spatial resolutions. The most important information about the three versions of the model – denoted as Model **MA**, Model **MB** and Model **MC** – are given in Table 1.

The resolution of Model **MA** in the southern Baltic Sea area corresponds approximately to 1Nm. Information about division of water column into the σ-layers is given in Table 2.

Bottom topography for the model was obtained from the data from the Institut für Ostseeforschung, Warnemünde [19]. The model was initialized on the basis of month-averaged data of temperature and salinity in the Baltic Sea, from years 1970–1990, collected

Table 1. Spatial and temporal resolution of the three versions of the model

	$\Delta x \times \Delta y$	kb	Δt_e	Δt_i	geographical area
Model **MA**	2'×1'	20	6s	180s	09°30'÷21°30'E; 53°50'÷57°10'N
Model **MB**	6'×3'	20	6s	180s	09°30'÷30°00'E; 53°50'÷65°50'N
Model **MC**	10'×5'	20	30s	900s	09°30'÷30°00'E; 53°50'÷65°50'N

Table 2. Values of the vertical coordinate (σ_i) and thickness of corresponding layers ($\Delta\sigma_i$), as defined for all three versions of the model

i	σ_i	$\Delta\sigma_i$	i	σ_i	$\Delta\sigma_i$
1	0.000	0.008	11	–0.438	0.063
2	–0.008	0.008	12	–0.500	0.063
3	–0.016	0.016	13	–0.563	0.063
4	–0.031	0.031	14	–0.625	0.063
5	–0.063	0.063	15	–0.688	0.063
6	–0.125	0.063	16	–0.750	0.063
7	–0.188	0.063	17	–0.813	0.063
8	–0.250	0.063	18	–0.875	0.063
9	–0.313	0.063	19	–0.938	0.063
10	–0.375	0.063	20	–1.000	0.000

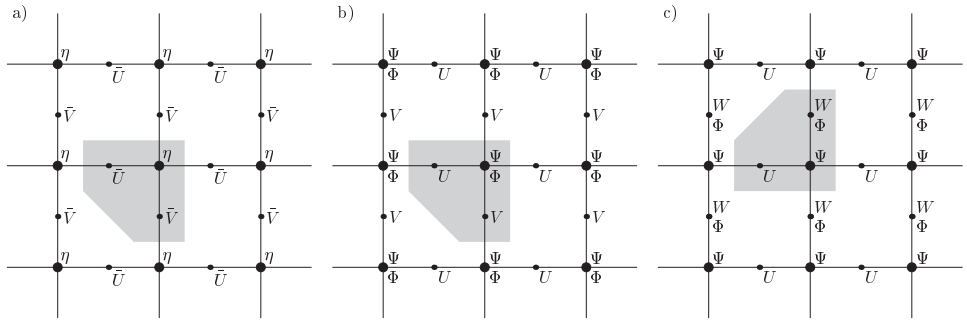

Figure 5. Numerical grid used in the external (a) and internal (b) and (c) mode. Ψ denotes T, S or ρ, Φ – K_M, K_H, q^2 or $q^2\ell$. Grey areas mark the positions of grid points with the same values of grid indices

in the Baltic Environmental Database (BED), and interpolated onto the model grids with the Data Assimilation System [20].

4. Diagnostic calculations

The first stage in applying POM to modeling the circulation in the Baltic Sea were diagnostic calculations, based on time-independent fields of water temperature and salinity, representative for a particular season.

Although the main purpose of diagnostic calculations was to provide initial conditions for the subsequent prognostic calculations (together with boundary conditions for the Model **MA**), they gave also a general idea of the main features of currents field, given the wind conditions.

The diagnostic calculations were carried out separately for each of the model versions, for each one of the four main wind directions, namely westerly, northerly, easterly and southerly wind. The value of surface wind stress was constant in space and time and equal to $1.0 \cdot 10^{-4}$ N·m^2. As a measure of equilibrium state the changes of free surface elevation were chosen. These changes were analyzed in several points of the computational grid with a time step of 30 minutes. Example diagram of such changes (for the westerly wind) is depicted in Figure 6. Fluctuations of the free surface elevation decline after about 10 days. Very similar results were obtained for the remaining three wind directions, for each of the model versions. Thus, an assumption was made that 15 days is enough time for the system to reach equilibrium state.

The results of simulations show that surface circulation is dominated by the Ekman transport modified by the shape of coastlines and bottom topography. The main features of this circulation are resolved – although with different accuracy – by all the three model versions. Along the coasts parallel to the wind direction intensification of the flow can be observed and strong currents (coastal jets) are formed. They are about 20 kilometers wide, which is in conformity with known observations [12]. Currents of this type are particularly characteristic for the Polish coast and reach a maximum speed during long periods of westerly winds.

An interesting feature of the Baltic Sea circulation is an existence of some stable current structures, almost independent of the wind conditions. A good example of such a structure is a mesoscale eddy in the area of the Gdansk Deep, strongly associated with a frequent occurrence of upwelling and downwelling events (they are manifested by a characteristic bend of salinity and temperature isolines [21]. This eddy is usually cyclonic and that is why upwellings dominate over downwellings in the discussed region. A second example can be a disturbance in the coastal jet in the area of Stolpe Bank (the effect of a sudden change of water depth).

The circulation in deep layers is in a good agreement with known results of observations (*e.g.* measurements made in the Bornholm Channel show that in its central part currents have direction opposite to the wind, [22]) as well as with results of other models. The structure of flow through the Stolpe Channel seems to favor a hypothesis of Krauss and Brügge [9] that the transport of water below the Ekman layer is opposite to the wind direction. This hypothesis was based on the results of a barotropic model (the authors assumed time-independent and ideally horizontal stratification so as to eliminate density currents) and thus it is not surprising that the structure of velocity field resulting from the POM calculations is more complicated. It is well known that this structure is particularly complex in the case when barotropic and baroclinic factors act in opposite directions – a good example is flow through the Stolpe Channel during winds from the west sector.

In the enclosed figures (Figure 8), which present model results along vertical sections the positions of which are depicted in Figure 7, it can be seen that in some cases the flow is almost depth-independent; such results have been obtained mainly for the spring stratification, when water masses are well mixed and density-driven circulation is very weak.

The maximum transport to the east occurs during periods of winds acting from the north; maximum transport to the west – during periods of winds from the south. The asymmetry of flow is caused by the Coriolis force. The strongest current is shifted to the southern part of the Channel during the flow to the east and vice-versa: the flow to the west

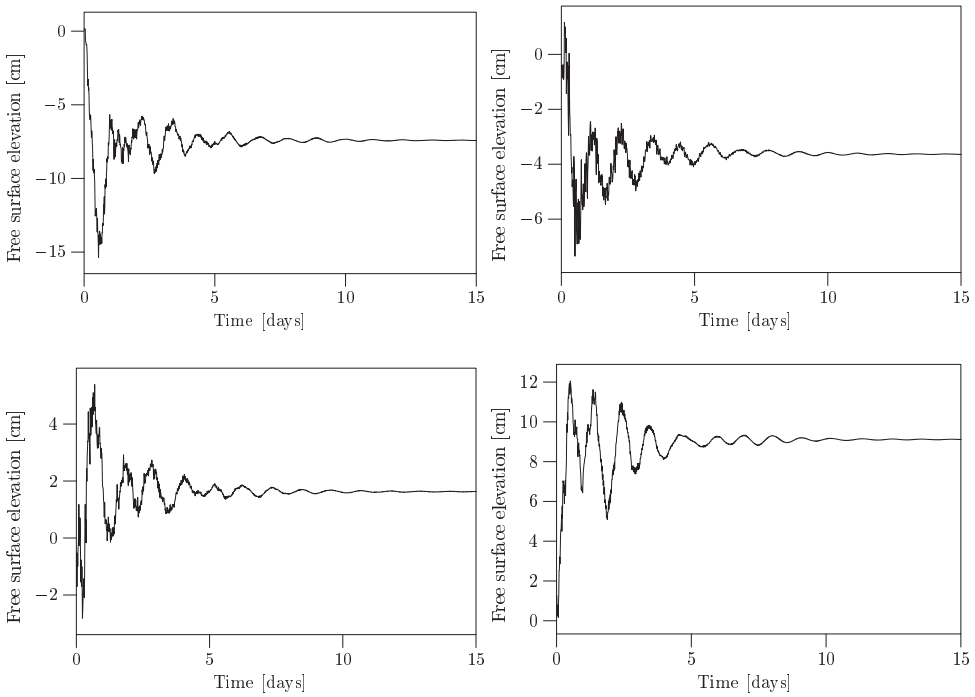

Figure 6. Changes of free surface elevation on chosen locations in the Baltic Sea, as an effect of a constant westerly wind (results of Model **MC**): in the Arkona Basin (upper left), in the Stolpe Channel (upper right), in the Gulf of Finland (lower left), in the northern part of the Gulf of Bothnia (lower right)

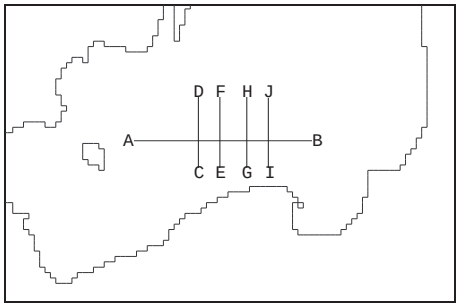

Figure 7. Position of sections in the Stolpe Channel area, along which the vertical structure of flow and salinity was analyzed

results in a displacement of maximum velocities to the north. This asymmetry is particularly strong in the western, narrowest part of the Channel.

The next section contains a more detailed description of flow through the Stolpe Channel, based on the results of prognostic calculations.

5. Prognostic calculations

As it was said in the introduction, the main purpose of this study was an analysis of the influence of spatial resolution of the model on the transport of water through the Stolpe

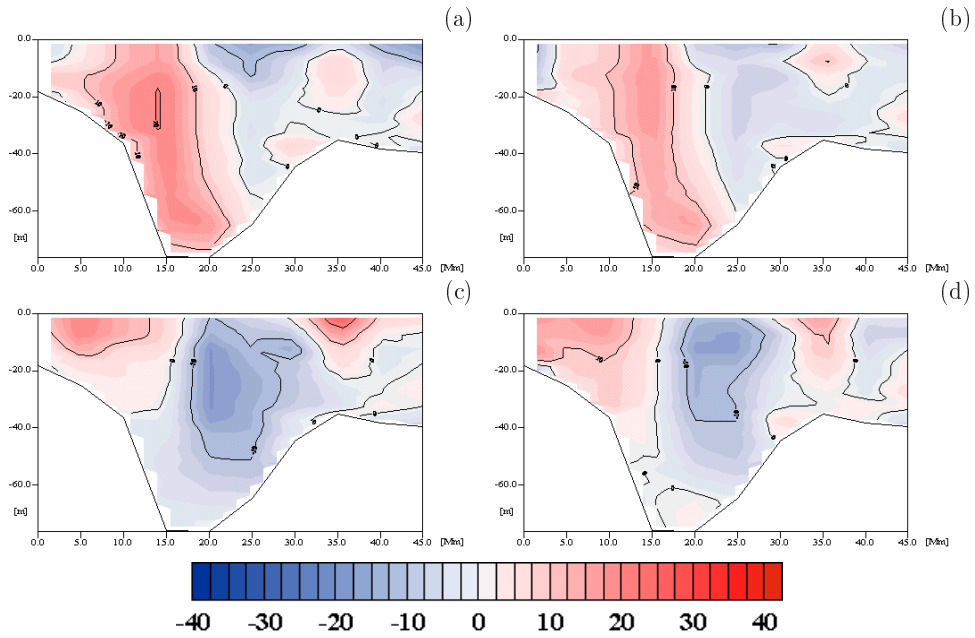

Figure 8. Vertical structure of velocity component parallel to the Stolpe Channel axis (in cm/s) on section CD under a northerly (a), easterly (b) , southerly (c) and westerly (d) wind. Negative values (blue) denote flow to the west

Channel. The basis of this analysis were prognostic calculations, carried out for variable in time, but spatially homogeneous wind conditions (Figure 9), for four main wind directions and three versions of the model. The changes in wind speed were chosen in such a way that they allowed, firstly, to observe hydrodynamic processes in the Stolpe Channel region under influence of sudden, strong wind impulse, and secondly, to analyze the behaviour of the system after ceasing of driving force.

The main parameter, on the basis of which an interpretation of water masses displacements was done, was transport (in m^3/s) across sections perpendicular to the axis of the Stolpe Channel, calculated separately for salty bottom waters and surface waters. As the boundary between the two water masses isohaline 10 PSU was chosen. Additionally, changes in vertical structure of water column were analyzed.

Attempts to estimate water transport through the Stolpe Channel and to understand the processes regulating it have been made by many researchers before. Table 3 contains some results, obtained either on the basis of measurements, or theoretical and numerical models. As can be seen, the values of estimated transport change from about 10 thousands m^3/s to over 100 thousands m^3/s. These differences are partly a result of different methods used, and partly a result of different criteria of classification of water masses. Additionally, investigations made on the basis of averaged, multiyear data may lead to different conclusions than those based on data collected in short periods of time (salinity measurements suggest that the transport below the halocline has a strongly episodic character, [23]). As will be shown below, the results obtained in this study are in the range of values from Table 3.

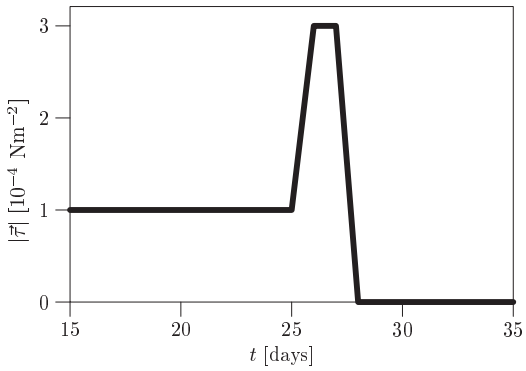

Figure 9. Changes of the modulus of surface wins stress $|\vec{\tau}|$ in the prognostic model

Table 3. Transport of water through the Stolpe Channel as estimated by different researchers on the basis of measurements and modeling. For details see the cited papers

Water transport through the Stolpe Channel estimated by different authors	
Rydberg, [24]	about 50000 m^3/s (for water of salinity over 8.5 PSU)
Pedersen, [25]	from 23000 to 54000 m^3/s; average: 34000 m^3/s
Omstedt, [26]	about 100000 m^3/s
Krauss & Brügge, [9]	for northerly winds:
	20 km^3/day in bottom layer,
	40 km^3/day in remaining layers;
	for easterly winds half of those values
Kõuts & Omstedt, [13]	average for years 1970–1990: 33000 m^3/s
Elken, [27]	average for years 1979–1994: 10900 m^3/s
	average for years 1987–1990: 6800 m^3/s
	(transport below 46 m depth)
Jakobsen, [28]	up to 100000 m^3/s
Paka et al., [29]	15000–17000 m^3/s

Diagnostic calculations described in the previous section suggested that in the Stolpe Channel two qualitatively different circulation patterns occur. Their development depends on the wind direction: northerly and easterly winds generate flow directed to the east, westerly and southerly winds – in the opposite direction. Prognostic calculations confirm this hypothesis and allow also to analyze changes in thermohaline structure of water column that accompany them.

5.1. Easterly and northerly winds

Surface layer circulation generated by easterly wind is almost identical in all three versions of the model (but of course different in terms of precision). Strong, directed to the east flow through the Stolpe Channel is a dominant feature of this circulation in deeper layers. In the case of Model **MB** and **MC** this is a flow of almost homogeneous structure,

connected with slight shift of the halocline and increase of salinity near the bottom of about 2 PSU in the period of the maximum wind velocity. Isohalines are displaced downwards to the right and upwards to the left (when looking downstream). This is a very characteristic feature of channel flow, explained by Ekman's theory, and was observed many times (*e.g.* 23–25). At the same time the most saline waters are shifted to the northern part of the Channel. After the wind ceases, flow velocities decrease and the stratification returns to its almost horizontal shape.

A different circulation pattern was a result of Model **MA**; in the central part of the Stolpe Channel an eddy developed, preventing the water to penetrate further to the east (Figure 10). It can be also seen that the flow has bidirectional character: apart from the main flow directed to the east there is also an area where water flows in the opposite direction. This quite complicated flow structure is accompanied by strong transformation of stratification. The Channel is filled with water of medium salinity (about 9–11 PSU), originating from the horizontal advection from the Bornholm Basin (Figure 11).

Quantitative comparison of the three model versions is given in Figure 12. In each case a strong peak of water transport during period of strongest wind can be observed in both surface and bottom layers. In the surface layer transport values are similar in each version of the model; the transport in the bottom layer is twice as big in Model **MA** than in Model **MB** and **MC**. These differences can also be seen by means of an analysis of water salinity – near the bottom and 5 m over the bottom salinity is bigger in Model **MA** than in the other two versions. The difference reaches over 2 PSU in the period of the strongest wind.

The processes that take place in the Channel during northerly winds are very similar to those described above. Flow velocities reach greater values, in both surface (over 40 cm/s) and bottom layer (over 20 cm/s). Water movement near the western entrance to the Channel has a character of typical inflow (Figure 13) of maximum intensity in periods of the strongest winds (27^{th} day of simulation). The transport of bottom and surface waters is similar in all three versions of the model.

5.2. Westerly and southerly winds

A completely different circulation develops as a result of the influence of wind from south-west sector. The currents during the period of maximum velocity of westerly wind are depicted in Figure 14, exemplified for the case of Model **MA**. Coastal jet, directed to the east, reaches in such conditions its maximum velocity, exceeding 1 m/s close to the Hel Peninsula. Very typical are also intensive mesoscale eddies of big vertical extent east of the Bornholm Island (in the left sides of Figure 14); they are of permanent character, lasting even a few days after ceasing of the wind, and have about 40 kilometers in diameter.

Surface water transport is compensated by directed to the west transport through the Stolpe Channel. Water flows to the Channel from the Gdansk Basin as well as from the Gotland Basin (through the Hoburg Channel). In the bottom layer a counteraction of barotropic and baroclinic processes takes place, and the resultant direction of water movement depends on horizontal salinity gradient on one hand and wind speed on the other hand.

The eddies close to the western entrance to the Stolpe Channel, mentioned above, are an effective barrier for water transport, which is reflected in salinity structure – high salinity water is removed from the Channel and accumulates in the Bornholm Basin (Figure 15).

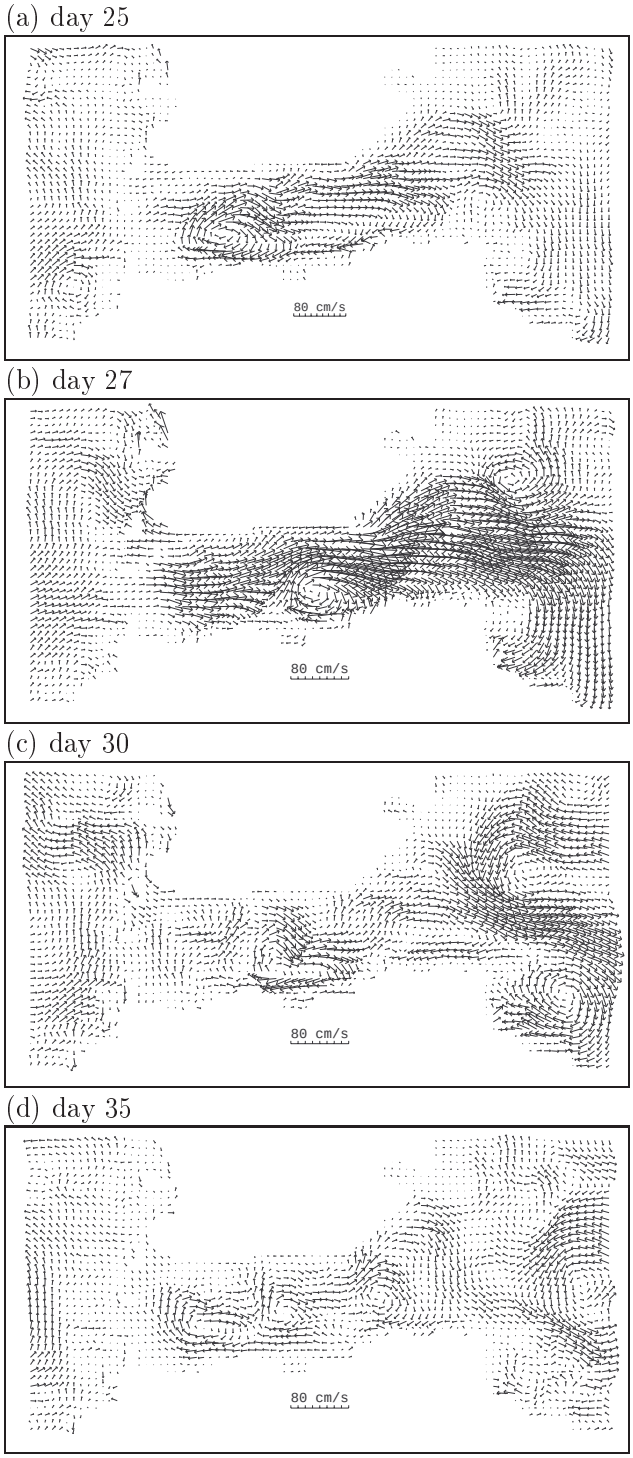

Figure 10. Currents in the Stolpe Channel at 60 m depth generated by easterly wind. Results of Model **MA**

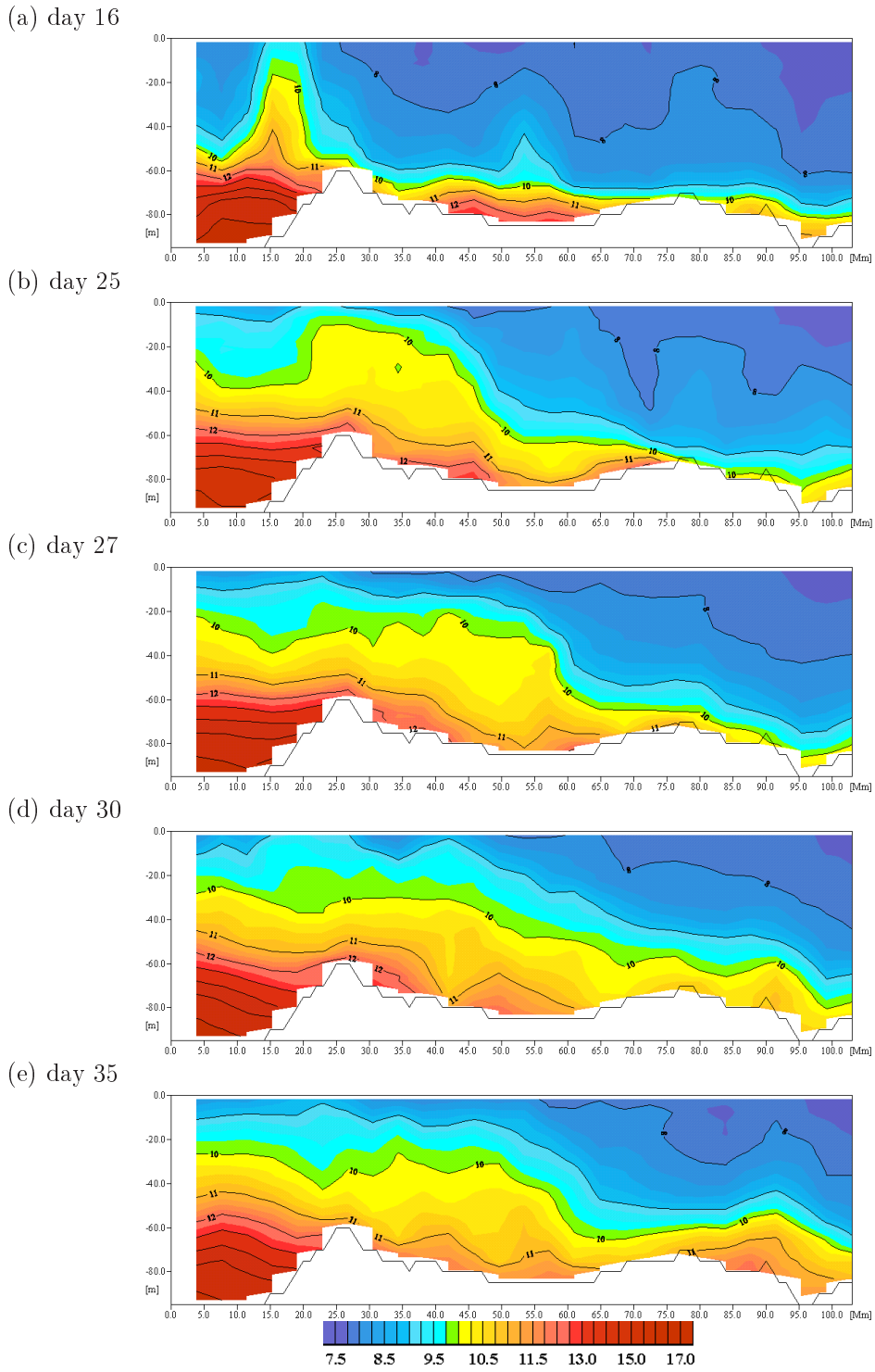

Figure 11. Vertical structure of salinity (PSU) along section AB under influence of easterly wind. Results of Model **MA**

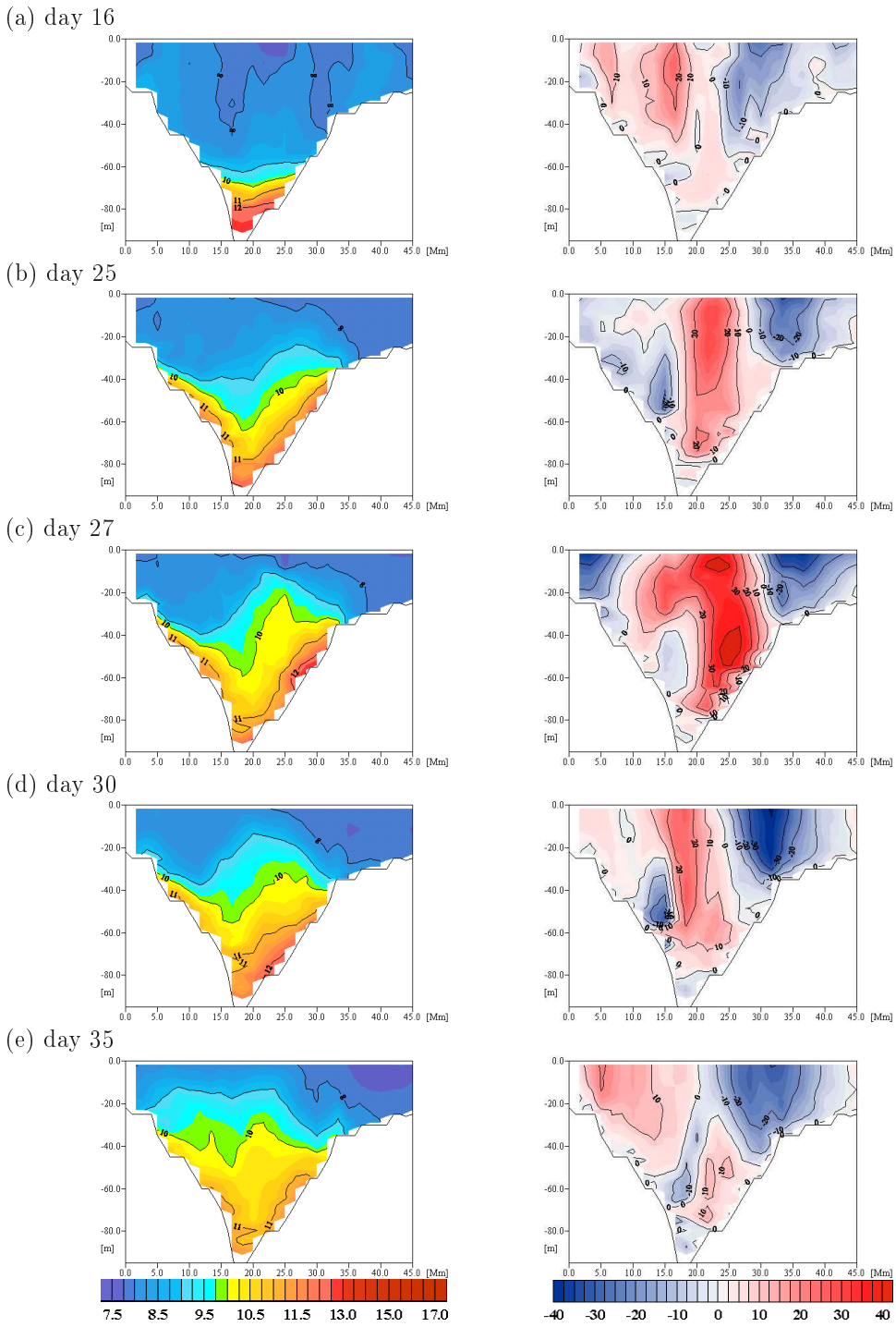

Figure 11 – continued. Vertical structure of salinity (left) and velocity (right) along section EF under influence of easterly wind. Results of Model **MA**

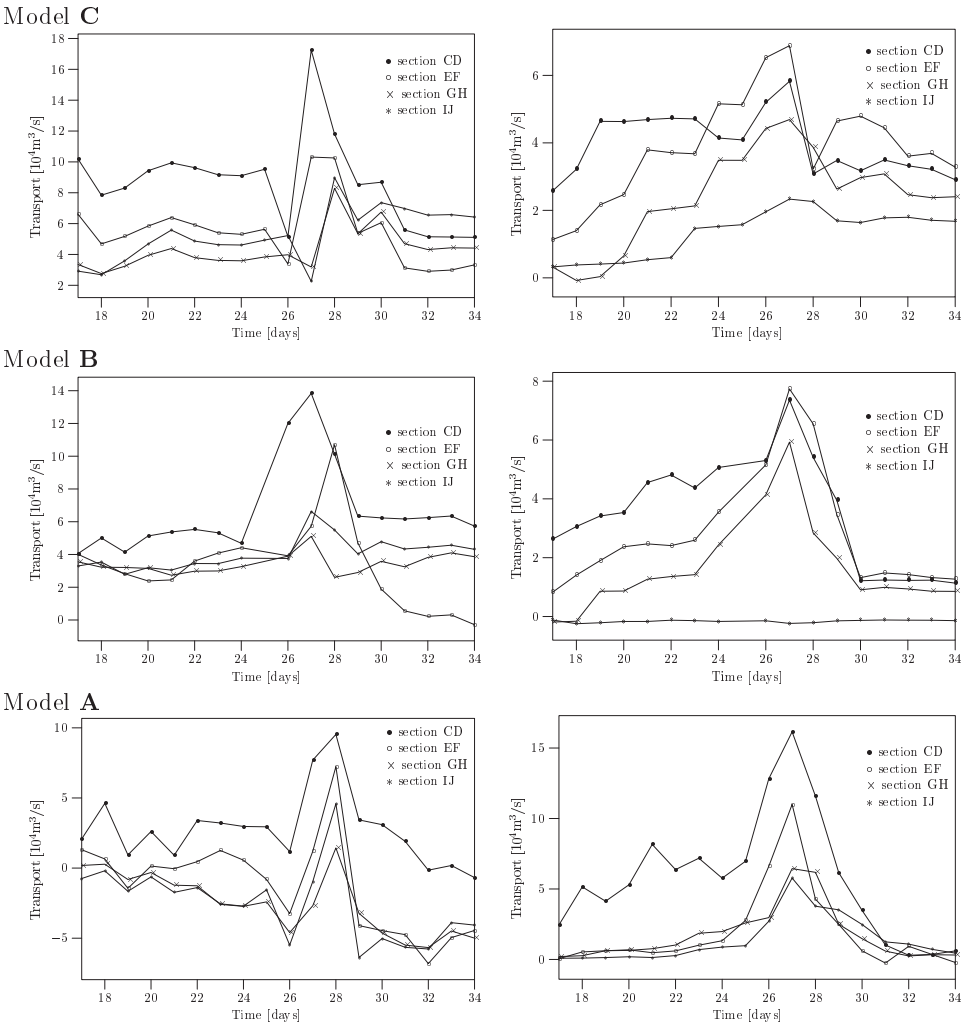

Figure 12. Water transport through the Stolpe Channel during easterly wind in the surface (left) and bottom layers, as a result of the three model versions

The above-mentioned conclusions cannot be drawn on the basis of the other versions of the model (the results of Model **MC** were almost identical to those of Model **MB**, depicted in Figure 16). The volume of high salinity water in the Stolpe Channel decreases, but the changes in salinity structure are not so strong as they were in Model **MA**.

From the point of view of refreshing the deep water of the eastern Baltic, southern winds are the most disadvantageous ones. During such wind conditions salty water is removed from the Stolpe Channel back to the west and low salinity water fills the entire volume of the Channel. The transport reaches its maximum negative values. It is worth to notice that after the wind ceases the flow very soon changes direction to the opposite (eastern) one and the volume of salty water in the Channel increases again. The barotropic component of the flow prevails only during periods of very strong winds.

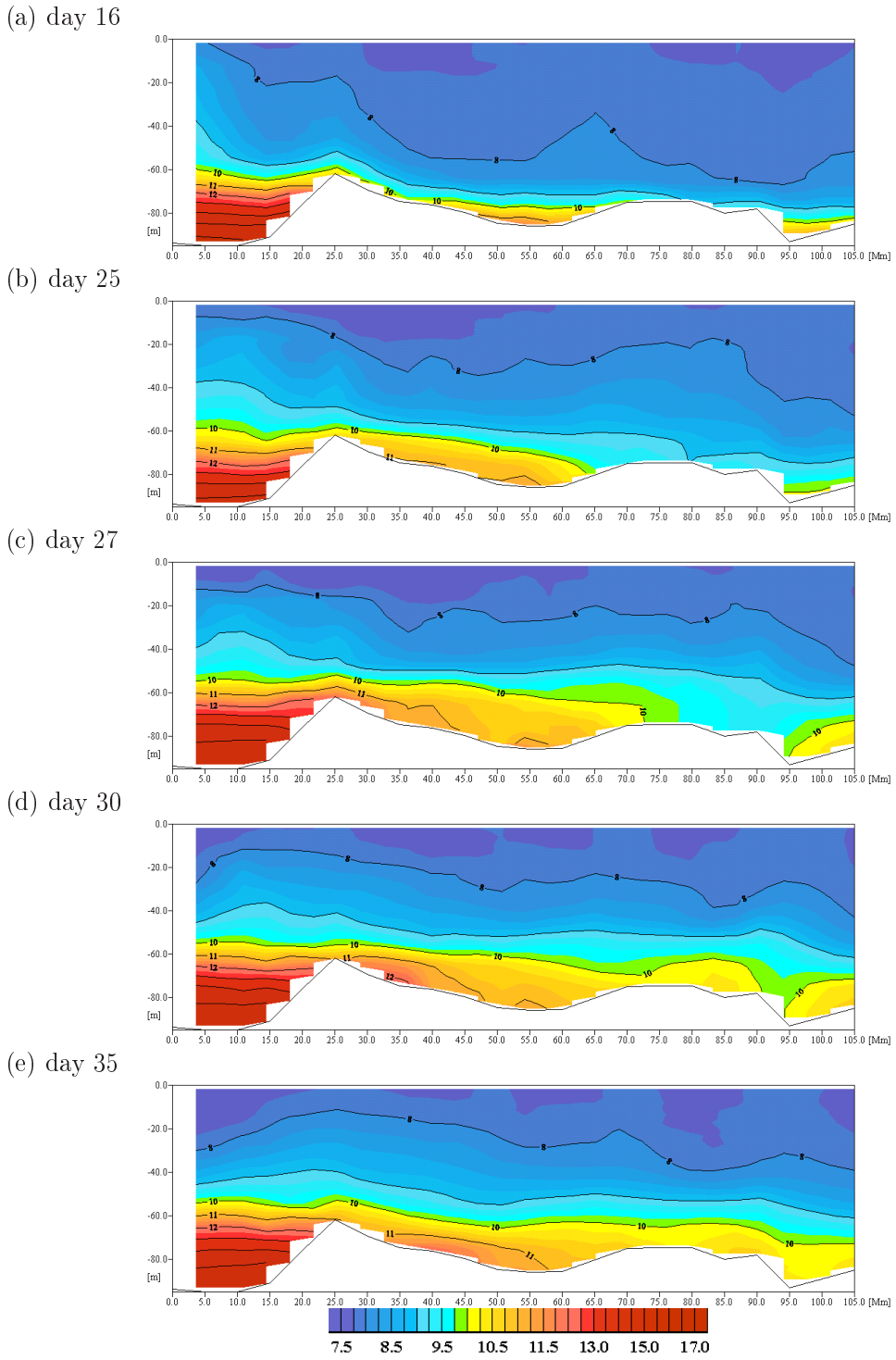

Figure 13. Vertical structure of salinity (PSU) along section AB under influence of northerly wind. Results of Model **MC**

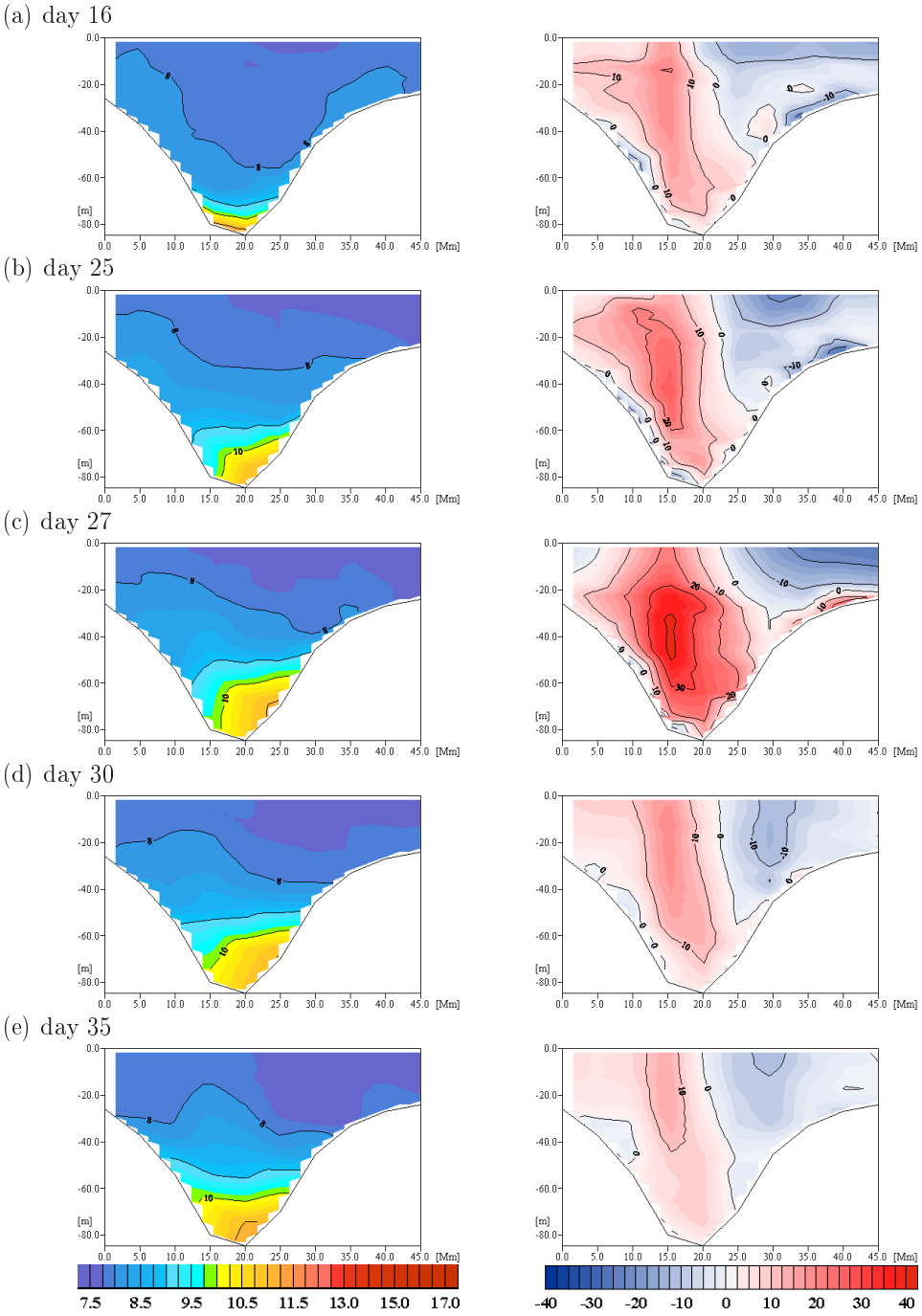

Figure 13 – continued. Vertical structure of salinity (left) and velocity (right) along section EF under influence of northerly wind. Results of Model **MC**

(a)

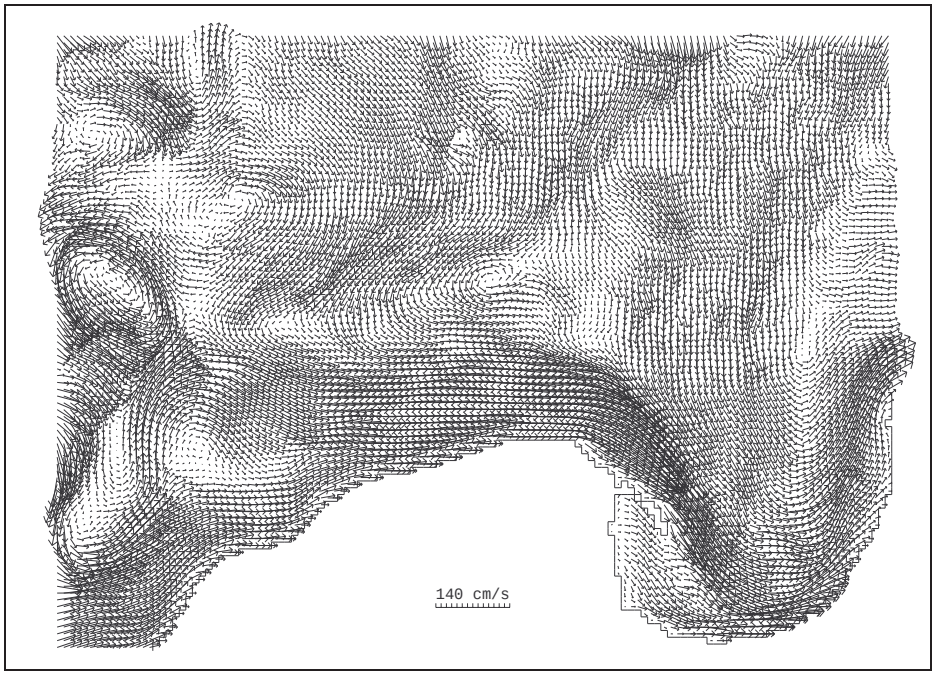

(b)

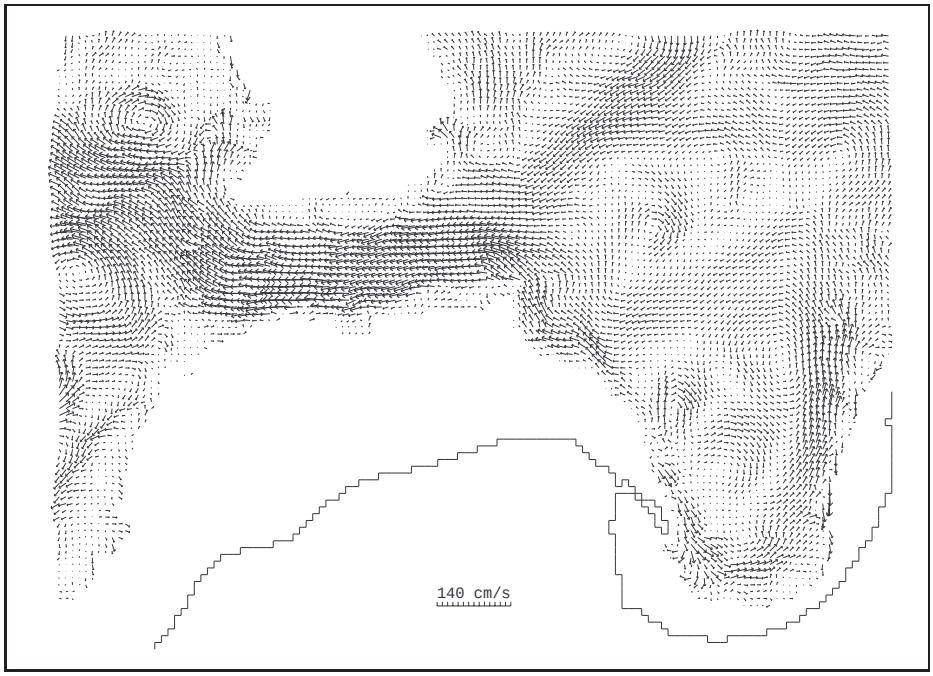

Figure 14. Currents in the southern Baltic Sea, generated by westerly wind; (a) – in the surface layer, (b) – at 60 m depth. Results of Model **MA**, 27th day of simulations

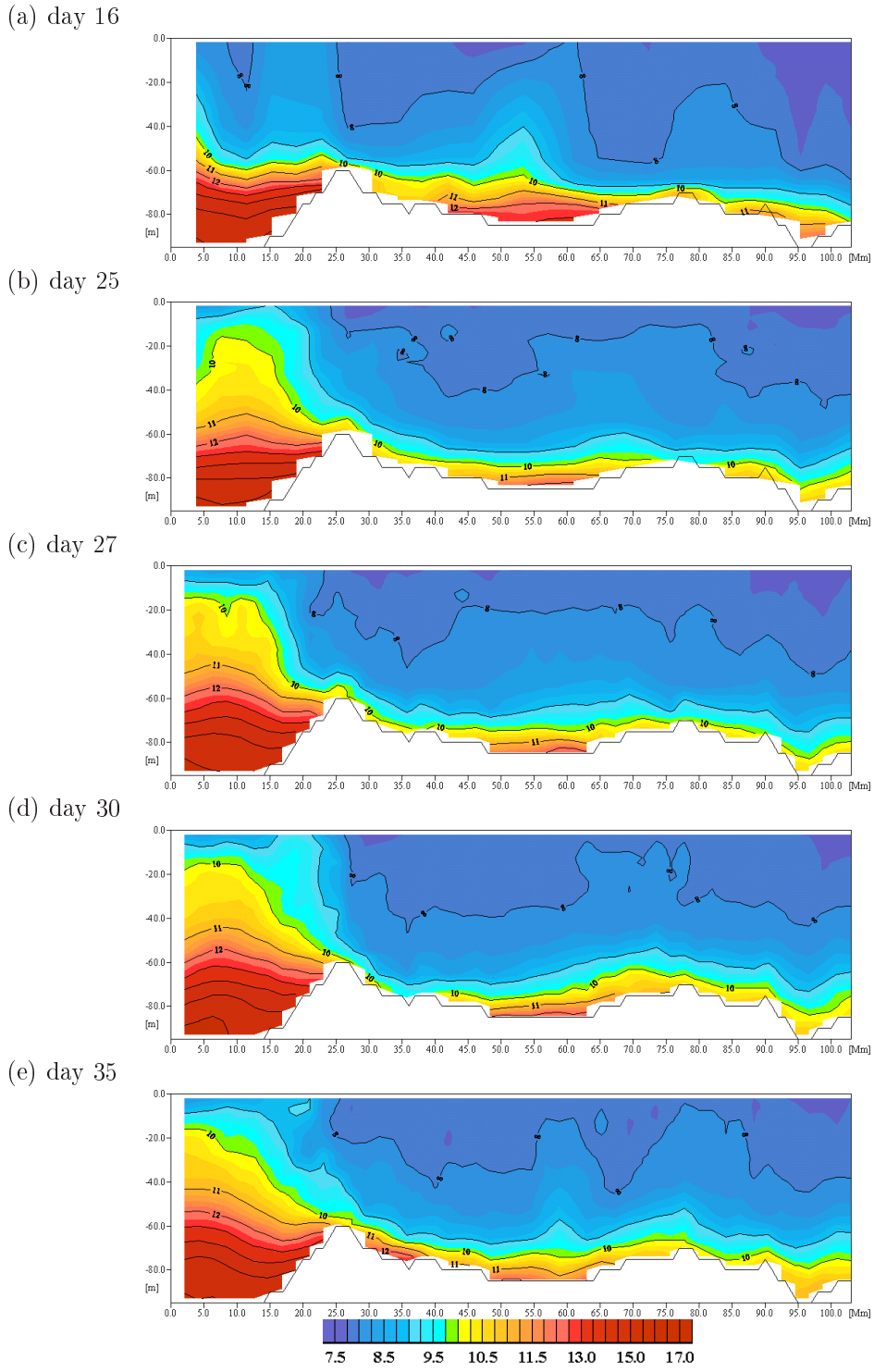

Figure 15. Vertical structure of salinity (PSU) along section AB under influence of westerly wind. Results of Model **MA**

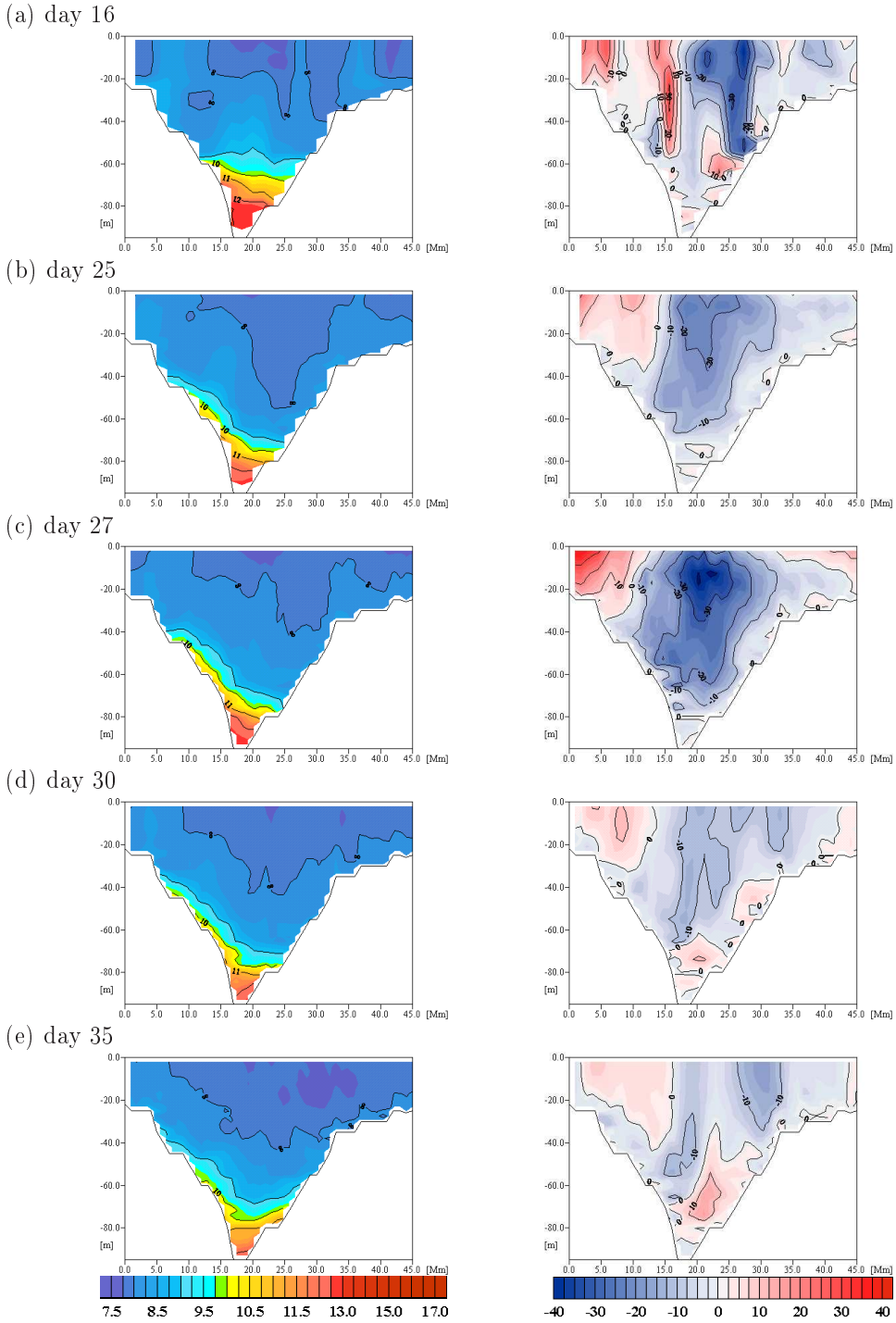

Figure 15 – continued. Vertical structure of salinity (left) and velocity (right) along section EF under influence of westerly wind. Results of Model **MA**

(a) day 16

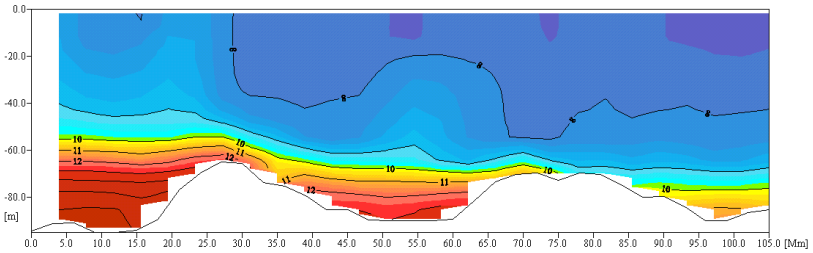

(b) day 25

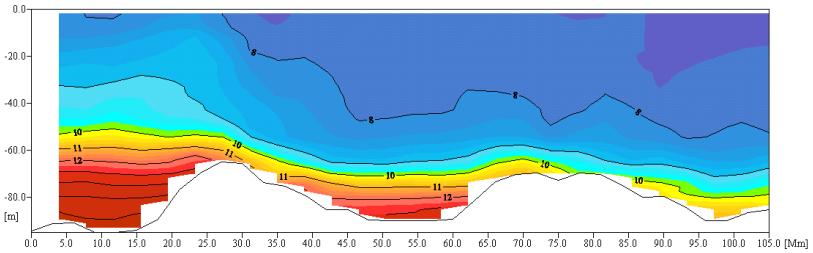

(c) day 27

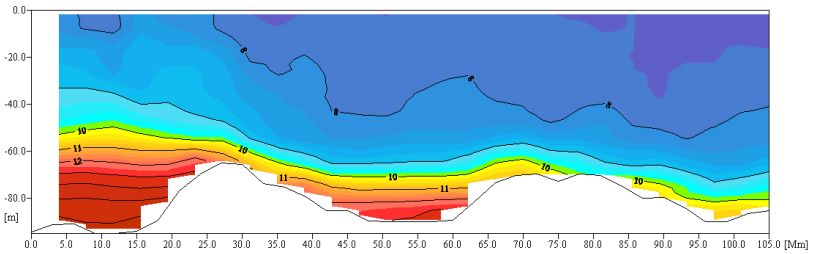

(d) day 30

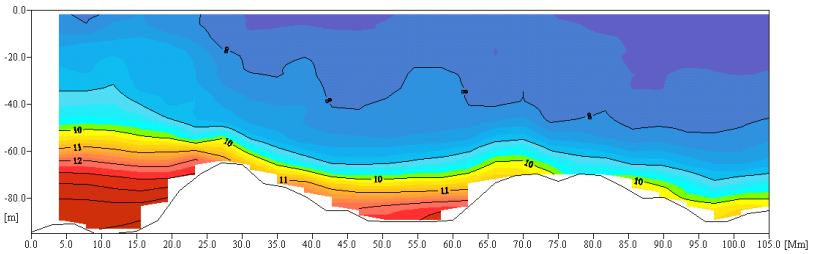

(e) day 35

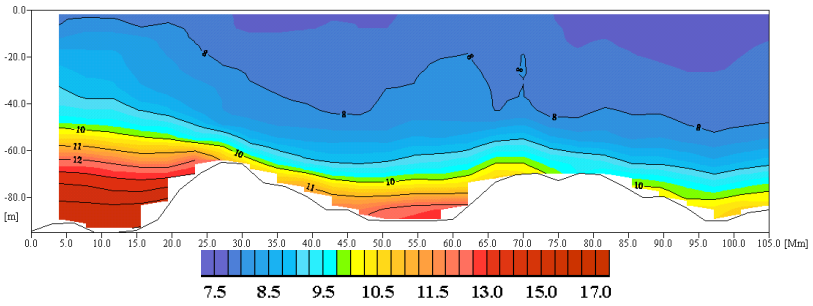

Figure 16. Vertical structure of salinity (PSU) along section AB under influence of westerly wind. Results of Model **MB**

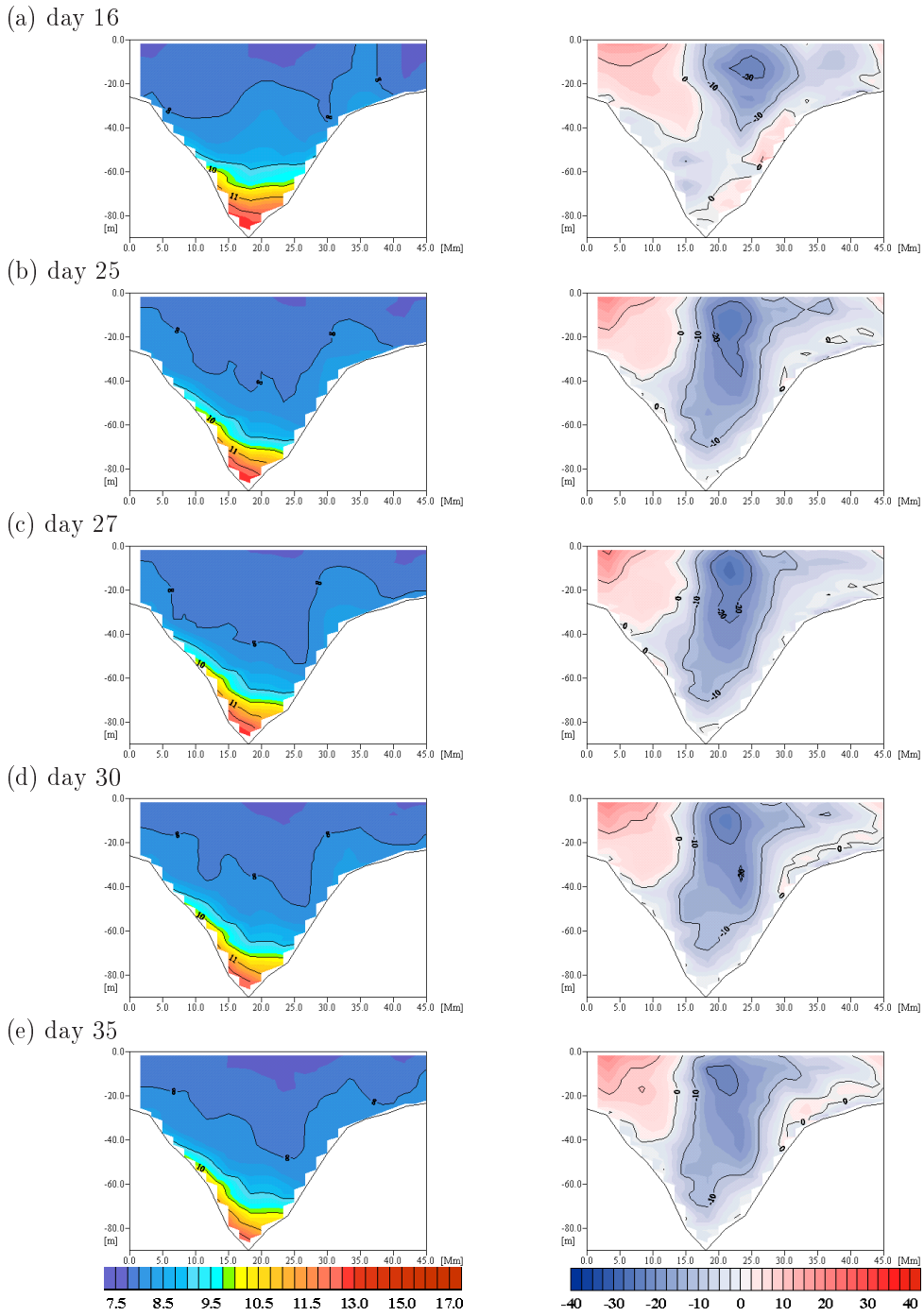

Figure 16 – continued. Vertical structure of salinity (left) and velocity (right) along section EF under influence of westerly wind. Results of Model **MB**

The calculations of the results which were described above were carried out for summer stratification. To check if they are representative for other seasons, experiments based on spring stratification were conducted. Their results did not differ in any significant aspect from those analyzed above. The reason for this is a fact that salinity, which shapes circulation in much higher degree than temperature, changes only slightly during the year (horizontal density gradient can be regarded as constant in all seasons).

6. Conclusions

The model results described in this paper make it possible to draw some general conclusions about dynamic processes taking place in the southern Baltic Sea. These processes are to a high degree dependent on local anemobaric conditions – barotropic component of flow shows high changeability correlated with changes of meteorological conditions. The reaction of the system for changes of driving forces is almost immediate – maximum flow velocity values occur in the periods of the strongest wind and decrease very quickly after its ceasing. In comparison to barotropic circulation, flow generated by horizontal pressure gradient (the effect of salinity differences) is constant, especially in bottom layers.

The results of the calculations confirm the hypothesis of Krauss and Brügge concerning relations between water transport through the Stolpe Channel and wind direction – the flow within the Channel is opposite to the wind direction on all depths except the surface Ekman layer. The only exception from this rule takes place in the situation when the wind-driven flow is directed to the west, but is not strong enough to oppose the density current directed to the east. Such a situation can occur during moderate wind from the western sector. The transport through the Stolpe Channel is accompanied by, known also from observations, characteristic changes in salinity structure (vertical movements and changes in the thickness of the halocline, inclination of isohalines *etc.*).

The comparison of the results obtained by three model versions of different resolution suggests that numerical grid step can have under some conditions a decisive influence on the circulation pattern being a result of the simulation. The differences in most cases are of quantitative character – they are revealed for example by over- or underestimation of the transport. In some situations however, when the structure of the flow is complex and strongly depends on bottom topography, its proper description is possible only when high resolution model is applied. In the Stolpe Channel area it is particularly important during westerly and easterly winds, where mesoscale eddies are generated and the flow is bidirectional. Such eddies – exerting influence on the net transport values – can be modeled only when in the Channel region suitable number of grid points are located. Coarse grid models tend in such cases to overestimate transport values. The results of Models **MA**, **MB** and **MC** are similar under northerly and southerly wind conditions, when flow is stronger and homogeneous.

When analyzing the results of experiments described in this study, one should remember that they were carried out on the basis of averaged multiyear data and with highly simplified boundary conditions (river input, processes of heat transfer between the sea and atmosphere, spatial variability of wind field were not taken into account). To answer a question how this simplification influences model results, a simulation based on real meteorological data would be required and detailed comparison with measured values of currents, temperature and salinity would have to be done. Such experiments are planned

for the nearest future in cooperation with the Institute of Oceanology PAS. Up to now it is only possible to state that the results are – in general meaning – in agreement with known results of other models and experimental data available. This is enough to realize the main purposes of the present study, namely to describe the main features of water circulation in the southern Baltic and analyze an importance of spatial resolution of the model.

Acknowledgements

The work was part of a research project No. 6 P04E 020 15, supported by the Polish State Committee for Scientific Research (KBN) in the years 1998–2000.

The authors would like to thank Dr. Torsten Seifert from the Institut für Ostseeforschung, Warnemünde, for providing bathymetric data of the Baltic Sea. We acknowledge also the authors of the Baltic Environmental Database, from which the salinity and temperature data was obtained.

References

[1] HELCOM 1996 *Third periodic assessment of the state of the marine environment of the Baltic Sea, 1989–1993. Background document*, HELSINKI COMMISSION, Baltic Marine Environment Protection Commission
[2] HELCOM 1996 *Third periodic assessment of the state of the marine environment of the Baltic Sea, 1989–1993. Executive summary*, HELSINKI COMMISSION, Baltic Marine Environment Protection Commission
[3] Jakobsen F 1995 *J. Marine Systems* no. 6 227
[4] Matthäus W and Lass H U 1995 *J. Phys. Oceanogr.* **25** (2) 280
[5] Boehlich M J 1987 *A three-dimensional baroclinic model of the Western Baltic*, in: Nihoul J C J, Jamart B M, *Three-dimensional models of marine and estuarine dynamics*, Elsevier Oceanography Series 45, ELSEVIER, Amsterdam–Oxford–New York–Tokyo
[6] Sayin E and Krauss W 1996 *Tellus* **48A** 324
[7] Fennel W and Sturm M 1992 *J. Marine Systems* no. 3 183
[8] Gidhagen L and Håkansson B 1992 *Tellus* **44A** 414
[9] Krauss W and Brügge B 1991 *J. Phys. Oceanogr.* **21** (3) 373
[10] Stigebrandt A 1987 *Tellus* **39A** (2) 170
[11] Omstedt A 1987 *Tellus* **39A** 254
[12] Lass H U and Talpsepp L 1993 *Continental Shelf Res.* **13** (2/3) 189
[13] Kõuts T and Omstedt A 1993 *Tellus* **45A** (4) 311
[14] Mellor G L 1998 *User's guide for a three-dimensional, primitive equation, numerical ocean model (1998 revision)*, 35 pp, Prog. in Atmos. and Ocean. Sci., Princeton University, Princeton
[15] Mellor G L and Yamada T 1982 *Rev. Geophys. and Space Phys.* **20** (4) 851
[16] UNESCO 1983 *Algorithms for the computation of fundamental properties of sea water*, UNESCO Tech. Pap. Mar. Sci.
[17] Jensen T G 1998 *J. Marine Systems* **16** (3–4) 297
[18] Engedahl H 1995 *Tellus* **47A** 365
[19] Seifert T and Kayser B 1995 *Meereswissenschaftliche Berichte* no. 9, Institut für Ostseeforschung, Warnemünde, p.72
[20] Sokolov A, Andrejev O, Wulff F and Medina M R 1997 *Systems Ecology Contributions* no. 3, Stockholm University, p.66
[21] Jankowski A 1996 *Oceanologia* **38** (4) 485
[22] Liljebladh B and Stigebrandt A 1996 *J. Geophys. Res.* **101** (C4) 8895
[23] Piechura J, Walczowski W and Beszczyńska-Möller A 1997 *Oceanologia* **39** (1) 35
[24] Rydberg L 1976 *Observations of the deep water flow through the Stolpe Channel during August 1976*, Institute of Oceanography, University of Gothenburg, Sweden, Report no. 15, 6 pp
[25] Pedersen F B 1977 *Nordic Hydrology* **8** 297

[26] Omstedt A 1990 *Tellus* **42A** 286
[27] Elken J 1996 *Deep water overflow, circulation and vertical exchange in the Baltic Proper*, Estonian Marine Institute Report Series, no. 6, Tallinn, 91 pp
[28] Jakobsen F 1996 *Deutsche Hydrographische Zeitschrift* **48** (2) 133
[29] Paka V T, Jurbas V M, Golenko N N and Stefancev L A 1998 *Fizika Atmosfery i Okeana* **34** (5) 713 (in Russian)
[30] Oey L-Y and Chen P 1992 *J. Geophys. Res.* **97** (C12) 20,063